applied sciences

MDPI

Article

CFD Simulation of a Temperature Control System for Galvanizing Line of Metal Band Based on Jet Cooling Heat Transfer

Giovanni Carozzo [1], Carlo Cravero [2], Martino Marini [3,*] and Matteo Mazza [1]

[1] Danieli Centro Combustion, Piazza Borgo Pila 39, 16129 Genova, Italy; g.carozzo@danieli.it (G.C.); m.mazza@danieli.it (M.M.)
[2] Dipartimento DIME—Università degli Studi di Genova, Via Montallegro 1, 16145 Genova, Italy; cravero@unige.it
[3] Dipartimento DADU—Università degli Studi di Sassari, Piazza Duomo 6, 07041 Alghero, Italy
* Correspondence: marini@uniss.it; Tel.: +39-079-972-0410

Received: 1 June 2020; Accepted: 27 July 2020; Published: 30 July 2020

Abstract: The work focuses on the development of a thermo-fluid dynamic simulation model of a section of close cooling, called a jet cooler, inserted in the galvanizing line of metal band production. Two models of increasing accuracy have been tested and calibrated by experimental data. Special attention to turbulence modeling and boundary conditions has been given. A literature survey was focused on the jet impingement process (the reference heat transfer mechanism for the system component) and on available correlations to predict the heat exchange coefficient. The numerical simulation of jet impingement has been applied to a module of an actual industrial cooler for steel band production. The operation of the jet cooler was simulated in real operating conditions to get a detailed insight into the jet impingement mechanism in order to optimize the heat transfer and reduce, as far as possible, the cooling fluid mass flow rate. The comparison of heat transfer correlations, used in industrial preliminary design, with detailed CFD results is discussed.

Keywords: CFD; jet impingement; heat transfer; galvanization process

1. Introduction

Jet impingement is a very efficient solution for cooling hot components, since very high heat fluxes can be removed. In many industrial processes, this cooling technique is used for the cooling of gas turbine blades, of electronic components, and the cooling process of metallic and glassy materials. In the galvanizing lines, it is necessary to quickly cool the steel before it enters the molten zinc bath. The temperature decrease in the metal, during the passage through close cooling sections, lies between 250 and 280 °C, and must be carried out with a certain rate that correlates with the mechanical characteristic of the steel under production and with the speed of the production line (production rate). A thorough study of this section of the system is of some importance; by optimizing the system, the overall dimensions can be reduced, as well as the electricity consumption of the fans.

The energetic optimization of industrial components in industrial plants with very high energy consumption, like steel or glass production systems, is of utmost importance to reduce both fuel consumption and pollutant emissions; a small percentage increase in efficiency can give relevant fuel and money savings. Even the tiniest effect in design improvement is therefore welcome. The use of CFD (Computational Fluid Dynamics) simulation can give a significant support to the development of industrial components where the heat transfer process is involved [1–3]. The effect of real gas flow can be also introduced [4] when severe expansion processes with a strong temperature gradient and heat transfer are involved, like in turbomachinery applications [5]. Over the years, several experimental

and numerical studies have been conducted both on single jets and on multi-jet systems. In the available literature, dealing with both experimental and numerical analysis, the effect of different parameters on the flow field and on the heat exchange properties at the wall was tested; the main parameters considered were: Reynolds number, distance between jet and wall, spacing between the jets, and geometry of the nozzle. Zuckerman and Lior [6] have reviewed the rich literature on the subject, reporting a number of empirical correlations developed by various authors for the prediction of the average Nusselt number on the surface to be cooled. Katti and Prabhu [7] experimentally investigated the effects of Reynolds number and of jet–wall distance on the heat exchange, for a single jet system, with a detailed study of the variation in the heat exchange coefficient along the radial distance from the jet axis. Geers [8] has experimentally tested the interaction of flows from multi-jet systems. The multi-jet configuration primarily affects the flow field, increasing the production of turbulent kinetic energy that determines the spatial distribution of heat exchange. The above solution is of particular interest to the present application and different simulations are discussed in the following sections.

On the numerical side, research applications (Behniaet al. [9]) have mainly studied axisymmetric jet impingement models, analyzing the influence of operating parameters and checking the validity of turbulence models in predicting both flow and thermal fields. Taking into account other studies from Bovo et al. [10], Thielen [11], Pattamatta et al. [12], Chougule et al. [13], and Wae-hayee et al. [14], it is clear that there is no single turbulence model that can be identified as the most effective for this physical phenomenon.

In the present work, the attention is focused on the heat transfer from a single jet or from a jet cluster to set up a proper CFD model for the analysis of the actual industrial configuration. Different test cases have been considered in order to have a proper insight into the flow mechanisms and to validate the proposed CFD approach. Initial simulations were performed on 2D axisymmetric models, comparing the results with experimental data from the literature and from the ERCOFTAC database [15]. Later, a 3D model was developed, with a matrix of 3×3 jets, using the data provided by Geers [16]. Finally, a section representative of the industrial jet cooler was simulated based on an actual configuration installed. The CFD results were also compared to those corresponding to a set of empirical correlations from the literature [6], which form the base for the industrial design process. The CFD approach can integrate the use of empirical correlations or support the calibration of specific correlations for a given product.

2. Numerical Simulations on Jet Impingement

2.1. Axisymmetric 2D Model

In order to compare the numerical results with the experimental investigations from the literature, two models of increasing accuracy are developed. The main geometrical parameters of the model are the vertical distance H from the jet nozzle exit to the wall and the nozzle diameter D. Geometries defined by H/D = 2 and 6 are considered with the same Reynolds number, referred to as the nozzle outlet:

$$Re = \frac{u_{mean} D}{\nu} \quad (1)$$

The Reynolds number is set at 23,000. The computational domain is made of a pipe of diameter D, a solid wall, an upper surface, and the outlet surface.

The pipe length is at least 10 D in order to guarantee a fully developed boundary layer at the jet outlet section. In Figure 1, the domain, with components and boundary conditions, is sketched. Structured meshes, generated using an ICEM-CFD package are considered, as shown in Figure 1.

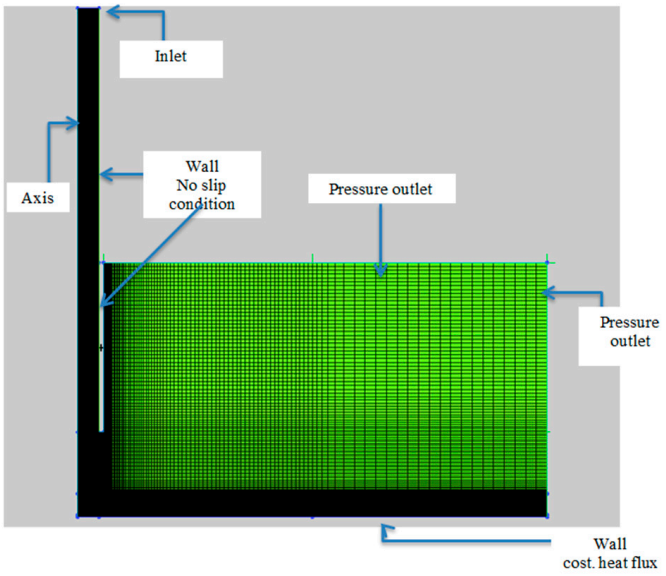

Figure 1. The 2D axisymmetric computational domain: case H/D = 2.

In Figure 2, the velocity contours are shown. In case the domain does not include the straight pipe, the jet velocity profile at the inlet boundary condition is obtained from a separate simulation of the flow in the isolated pipe. A constant heat flow is imposed along the wall and the atmospheric pressure is set at the outlet sections. According to the literature for similar applications, the v^2f turbulence model is selected. The analyses are set to steady flow with an upwind second-order spatial discretization. The simulation convergence is based on the stabilization for the wall temperature. The main heat transfer parameter is the Nusselt number:

$$Nu = \frac{hD}{k} \tag{2}$$

where h is the local or average coefficient of convective heat exchange, calculated as follows:

$$h = \frac{\dot{q}}{\left(T_{wall} - T_{jet}\right)} \tag{3}$$

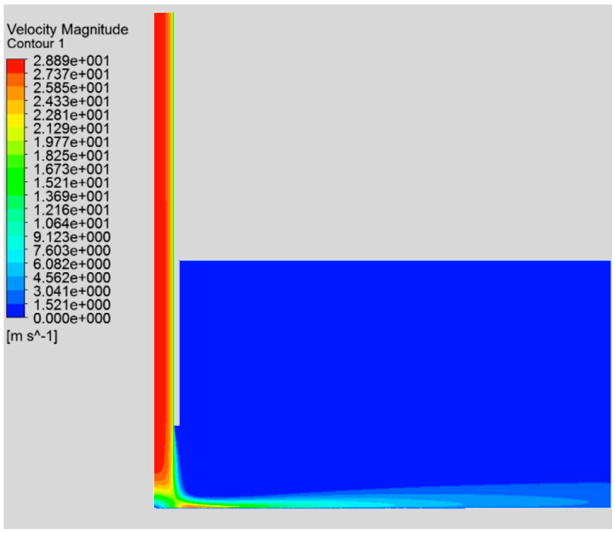

Figure 2. Velocity magnitude contours in case H/D = 2.

D is the nozzle diameter and k is the thermal conductivity of the evolving fluid (air). The values of air thermal properties (thermal conductivity and kinematic viscosity) are evaluated at the fluid inlet temperature. In Figures 3 and 4, the Nusselt number distributions on the wall for cases H/D = 2 and H/D = 6 are respectively shown. The Nusselt number distribution is plotted at distance r from the jet center using the non-dimensional variable r/D. A good match between the present numerical results and the experimental data provided by Yan [17] and Baughn et al. [18] is observed. The predicted heat exchange is underestimated with respect to the data from Katti et al. [7].

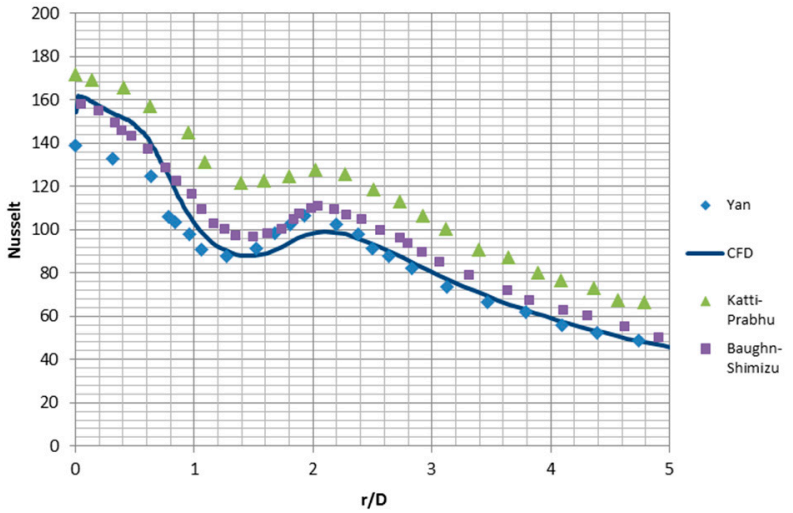

Figure 3. Nusselt number along the wall H/D = 2—CFD vs. experimental data.

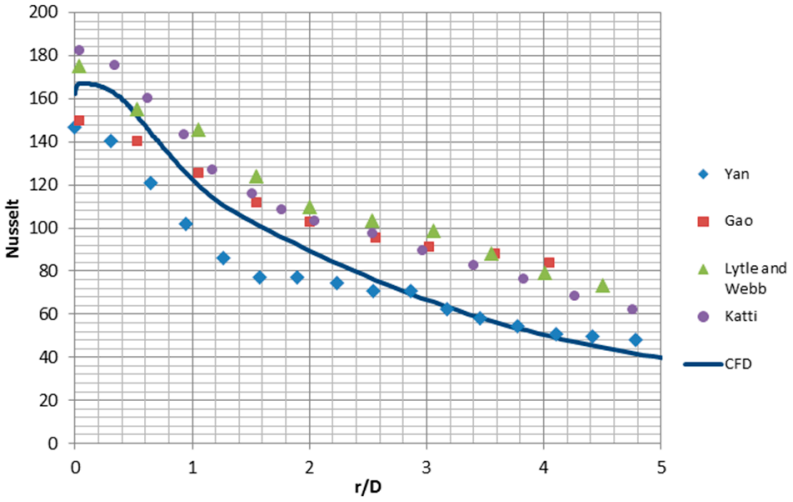

Figure 4. Nusselt number along the wall H/D = 6—CFD vs. experimental data.

2.2. 3D Model

To check the effects of the interaction among different jets, a 3D case is analyzed: it is characterized by nine in-line jets arranged in three rows. Geers [8] experimentally investigated the same geometry considered; in Figure 5, the top view of the geometry is shown. A perforated plate generates the jet cluster; the diameter D = 13 mm, the distance s between hole centers is 52 mm, and the jet–wall distance is H = 52 mm. The dimensionless ratios H/D = 4 and s/D = 4 are obtained.

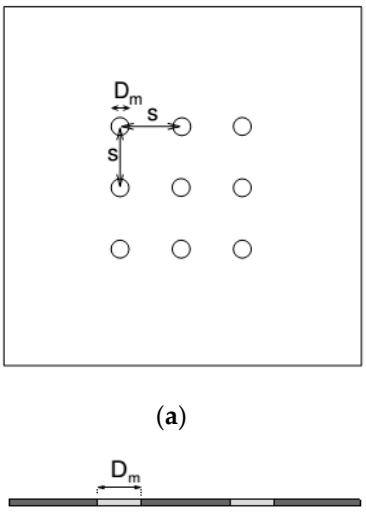

Figure 5. Geometry of the experimental analysis by Geers. (**a**) Top view and (**b**) side view.

Taking advantage of the geometrical symmetry, only a quarter of the actual geometry is modeled. The symmetry condition is imposed on the outer surfaces of the volume passing through the axes of the modeled jets. The inlet boundary conditions for jet velocity and turbulence profiles are obtained from a separate model that simulates the flow from the orifice. In Figure 6, an overview of the domain with the block-structured mesh is shown, and in Figure 7, the detail of the orifice mesh for the inlet velocity and turbulence profile is reported.

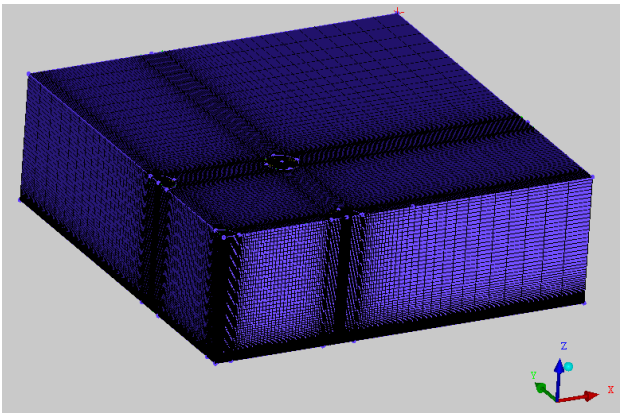

Figure 6. Geometric model for 3D case.

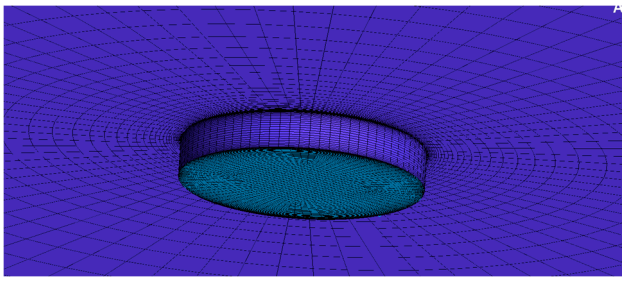

Figure 7. Detail of the geometry adopted to simulate the flow coming out of an orifice.

After a sensitivity analysis on the grid, to find the proper refinement, a mesh with about 1.1×10^6 elements is selected to give a value of $y^+ < 1$ at the wall. Three simulations are carried out, with the

same Reynolds number (Re = 20,000). The kinematic viscosity for the above Reynolds number is evaluated at the temperature of the jet. Different turbulence closures are compared for the 3D flow structure analysis: realizable k-ε (with the use of enhanced wall treatment), v^2f, and k-ω SST.

The jet reference temperature was chosen to compare the results with Geers' data; the thermal conductivity was also evaluated at the same temperature as in the Nusselt number calculation. A constant heat flux is set at the wall, and the pressure is set equal to the environment on the outlet surfaces. As in the previous case, the SIMPLE spatial scheme is used and the variability of the thermo-physical properties with temperature is considered. The first-order upwind discretization scheme is preferred over the higher order scheme because of its higher stability. Numerical instabilities arise with the higher order upwind scheme.

In Figure 8, the numerical results from the different turbulence closures are compared to the reference data. After a qualitative comparison based on the experimental and numerical contours, it can be noted that the realizable k-ε model provides the best results. In contrast to Behnia et al. [9] and consistent with Wae-Hayeeet al. [14] and Pattamatta et al. [12], for a 2D model, the realizable k-ε model can provide comparable or better results than the v^2f option. Such a difference, if compared to the 2D case, can be attributed to a higher robustness of the k-ε model, which is stronger and more stable, in obtaining the convergence and the wall temperature stabilization. Furthermore, the incoming turbulence is very different between a fully developed flow and the flow generated by an orifice. In the former, it is greater at the center of the jet, while in the latter, the turbulence is higher along the edges of the jet, because of the vena contracta formation. These different velocity and turbulent profiles give different jets from a physical point of view.

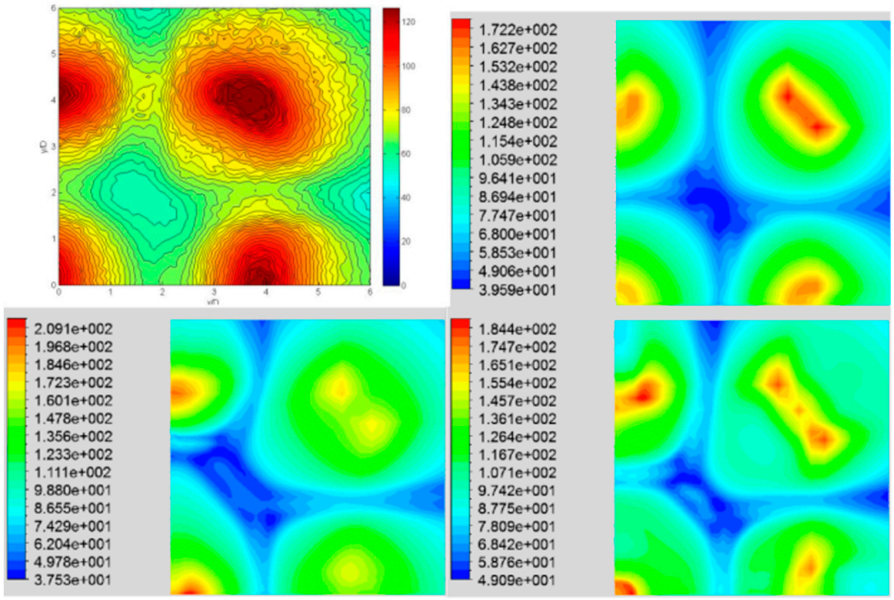

Figure 8. Nusselt contours for different turbulence models. Top left: experimental data by Geer. Top right: contours with realizable k–ε model. Bottom left: contours with k–ω SST model. Bottom right: contours with v^2f model. The variable x/D (0-6) in the abscissa, y/D (0-6) in the ordinates.

The turbulent profile from the orifice has lower values of turbulent kinetic energy on the jet axis. From a numerical point of view, this lower value of incoming kinetic energy gives a lower overestimation of k, typical of the k-ε model in stagnation zones.

In Figure 9a,b, the trends of the predicted Nusselt number distributions along the wall for x/D = 0 and x/D = 4 are respectively shown. They correspond to the planes passing through the axis centers of the jets. The above data are compared with the results from Geers [8]. The realizable model k-ε provides a linear distribution of heat exchange compared to the other models, showing a better match with the experimental data trend. All the turbulence closures considered give an overestimation of the

peak value. The k-ε is able to give a closer match with the reference shape with a lower overestimation of the Nusselt number compared to the other models. The peak value is largely overestimated (about 25%) but it occurs in a very small area close to the jet center with negligible effects on the overall heat exchange.

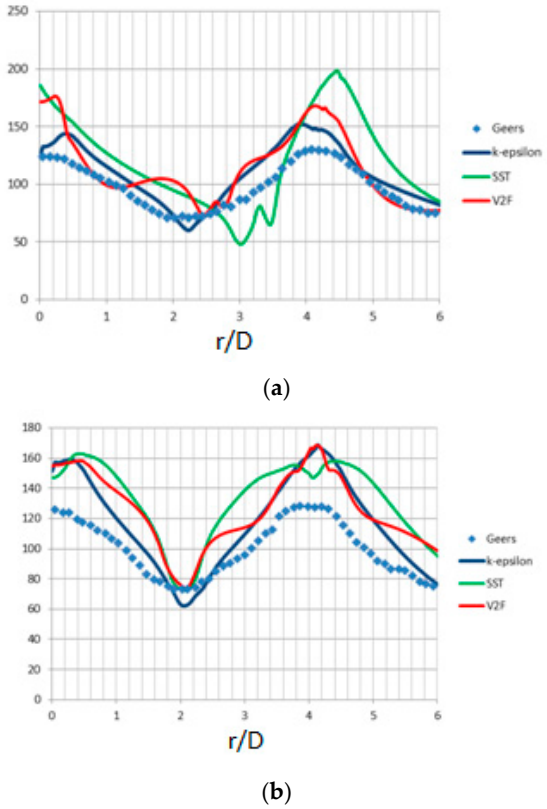

Figure 9. Experimental and numerical trends of the Nusselt number: (**a**) x/D = 0 and (**b**) x/D = 4.

In Figure 10, the velocity contours at plane x/D = 0 from the numerical simulation (above) and the experimental data (below) are compared. A difference is observed at the jet axis. Compared to the experimental case, the numerical data have a lower speed decrease on the jet axis. This may further account for the overestimation of the heat exchange in the stagnation area.

In Table 1, a comparison of various results is reported, based on the mean convective heat transfer coefficient on the wall. Such a parameter is selected because some correlations are based on a different reference temperature, i.e., the film temperature T_{film}, defined as follows:

$$T_{film} = \frac{T_{inlet} + T_{wall}}{2} \tag{4}$$

It is incorrect to compare Nusselt values calculated with respect to different temperatures; it is preferable to compare the heat transfer coefficient that is a physical quantity independent of the reference temperature selection.

The correlations of Huber and Viskanta [6] and Goldstein and Seol [6] were applied on the basis of both temperatures, since the available literature did not specify what the reference temperature was. The most accurate correlations are those proposed by Geers and by Milani. The error of the CFD results is about 10% with respect to an average value. This percentage is acceptable from an industrial design point of view. With the above positive results, the proposed CFD model for jet clusters can be considered a valid tool for the simulation of the industrial jet cooler module made of several jet clusters.

Table 1. Comparison of CFD, experimental, and numerical correlation [6] data.

	Nu (Average)	Convective Heat Transfer Coefficient h [W/m^2 K]	Percentage Error
Geers—exp	83.13	165.18	—
CFD	92.20	183.19	10.90
Correlations			
Geers (inlet)	81.20	161.39	−2.29
Milani (film)	289.58	158.88	−3.82
Floreschutz (film)	97.03	192.79	16.70
Huber-Viskanta (inlet)	90.01	178.84	8.27
Huber-Viskanta (film)	73.38	145.80	−11.73
Goldstein-Seol (inlet)	51.56	102.45	−37.97
Goldstein-Seol (film)	42.16	83.77	−49.29

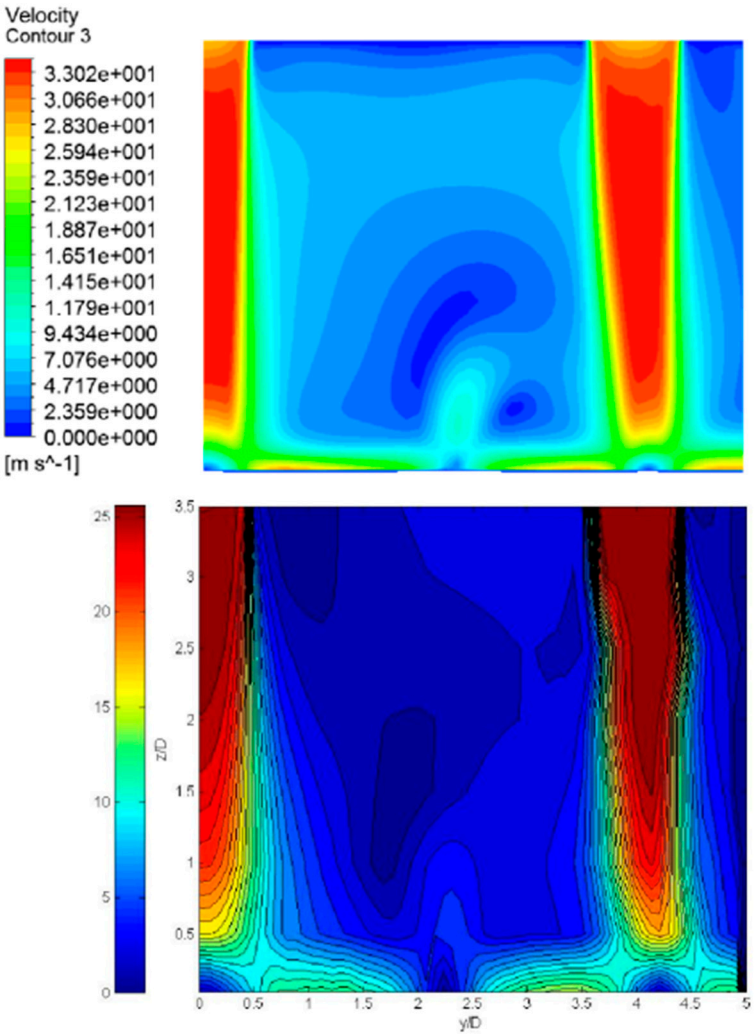

Figure 10. Velocity contours for the plane x/D = 0 (numerical above, experimental below).

3. Industrial Jet Cooler Module

3.1. CFD Simulation of the Module

A module of the industrial cooler is considered in the present paragraph. A sketch of the system is shown in Figure 11. Channels connecting the close cooling chamber with the pressure plenums generate the jets. The process fluid is a hydrogen–nitrogen mixture (HNX) to avoid oxidation of the surface of the metal sheet, and it is fed by a system of industrial fans. The hot fluid is cooled by means of a water heat exchanger and is then recirculated. In Table 2, the main geometrical data of the industrial cooler under investigation are reported. The pressure p_{jet} of the fluid at the inlet of the jets is given with respect to the jet diameter along the spanwise and streamwise directions.

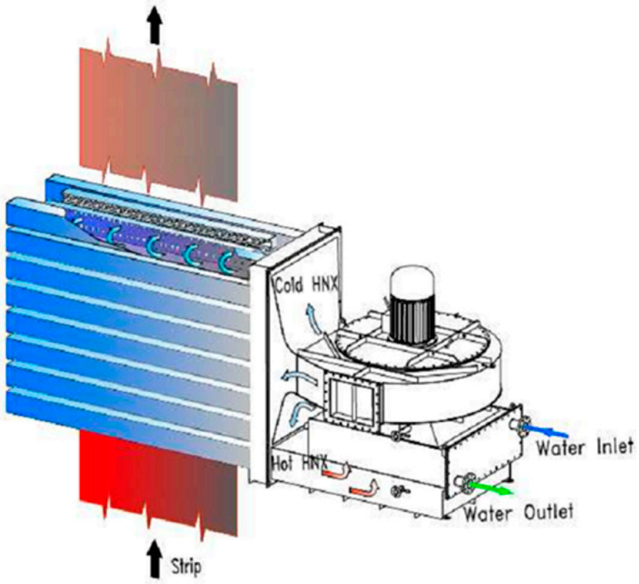

Figure 11. Schematic of the jet cooler system.

Table 2. Main geometrical data of the industrial cooling module.

H/D	6.250
$(p_{jet}/D)_{spanwise}$	6.875
$(p_{jet}/D)_{streamwise}$	6.250
Band thickness [mm]	0.680

A single module is composed of 256 jets, arranged in 16 staggered rows. Each row is displaced with respect to the previous one, in the direction of the jets, by a distance equal to a quarter of the drilling; every four rows of jets, the starting configuration is repeated. In Figure 12, the details of the arrangement of the holes are shown; the upstream and downstream parts of the complete geometry modeled are not shown in the figure. The metal band to be cooled moves at a constant speed in a direction parallel to the longitudinal sides of the model. Only a central section of the jet cooler is considered; periodicity conditions on the lateral surfaces, to reduce computation time, are introduced. Figure 13 includes a part in front of the holes and a suction mouth for the HNX (colored in red).

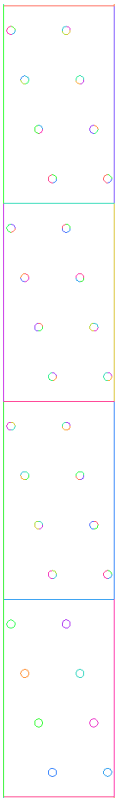

Figure 12. The 2D arrangement of holes.

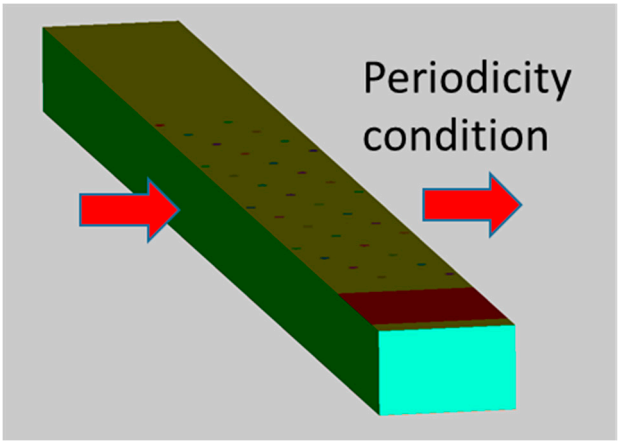

Figure 13. Overall 3D geometry.

Since the band is moving, the process is intrinsically unsteady. The frame motion option is selected and applied to the solid volume, i.e., the band. In this way, the temperature of the band at the inlet surface, equal to 660 °C, is set as a boundary condition on the wall, instead of a thermal condition on the surface hit by the jets. The temperature information propagates with a defined speed in the solid volume (set equal to the speed of the band). With this approach, it is possible to simulate the actual cooling of the band through a steady calculation. This input temperature is set up to simulate a jet cooler placed at the center of the line to set the flow periodicity without strong assumptions; the border effects at the entrance and the exit of the system are neglected. On the surface affected by the jets, the moving wall condition is enforced to correctly represent the flow drag due to the moving band.

As previously mentioned, the condition of periodicity is set on the lateral surfaces of the flow volume (as sketched in Figure 13) to take into account that such geometry represents only a module of

the entire jet cooler. With this hypothesis, the boundary effects due to the lateral side walls are also neglected. For the test cases, the jet input boundary conditions of the speed and turbulence profiles are obtained with a separate calculation, carried out on the geometry of the inflow duct to the chamber. In Figure 14, the detail of the plenum with the hole used to develop the jet in the present case is reported. The above model is used to obtain the velocity and turbulence profiles used as inlet boundary conditions for each jet of the module. A detail of the corresponding structured mesh is reported in Figure 15.

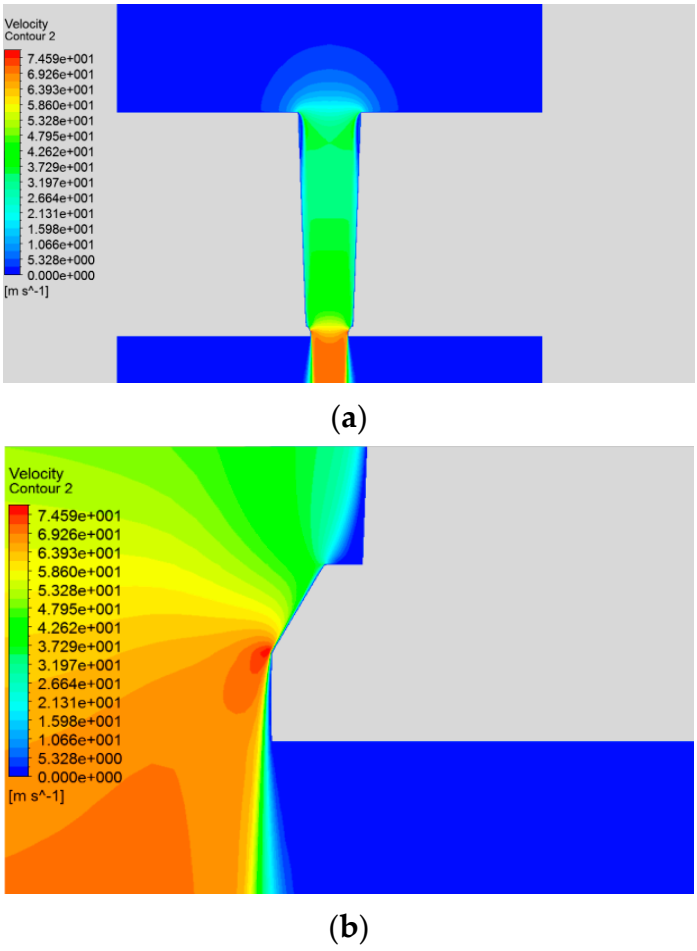

Figure 14. Velocity contours on the mid-section of the inflow duct. (**a**) Overall view and (**b**) detail of outlet section.

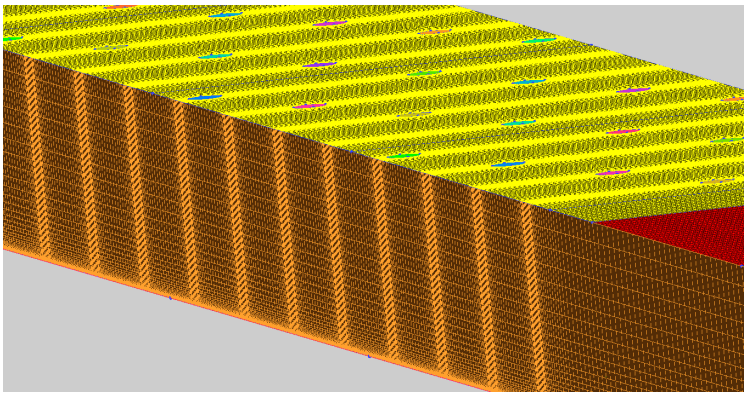

Figure 15. Mesh detail.

The outlet pressure of 100 Pa is set on the suction mouth (Figure 13). A symmetry condition is imposed on the lower surface of the metal strip, since in the real system, the jet coolers are located on both sides (upper and lower) of the strip, to ensure uniform cooling.

Based on the previous experience with the test cases, the turbulence model used is the realizable k-ε, with the option of enhanced wall treatment.

The discrete ordinate (DO) radiation model is activated to take into account the radiative heat transfer. The structured mesh has $7*10^6$ elements with a grid refinement to get $y^+ < 1$ at the wall. The metal band is also meshed and the conjugate heat transfer is considered to simulate the heat conduction mechanism into the band. In Figure 16, the streamlines through the modeled volume show the overall flow structure and highlight a correct repartition induced by the periodicity condition towards the suction mouth.

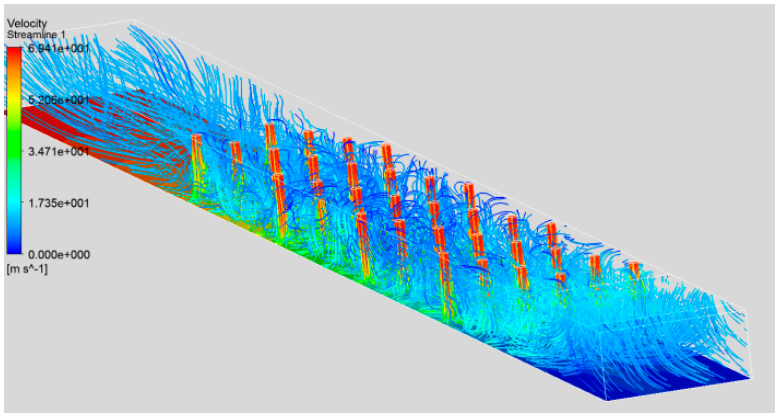

Figure 16. Streamlines in jet cooler model.

The distortion of the jets, in the streamwise direction, closest to the suction mouth can be clearly noticed in the side view shown in Figure 17. This situation affects the heat exchange in the area closest to the suction, with a reduction because the deflected jets do not correctly impinge on the band surface. In Figure 18, the surface temperature of the band is shown. The result obtained is comparable to the distribution due to a steady analysis; the temperature decreases from the inlet to the outlet of the computational volume. A higher temperature gradient can be seen in the area below the jets, as expected. The predicted ΔT between inlet and outlet is approximately 35 °C and matches the design intent for this specific jet cooler; this confirms that the simulation approach is representative of the actual solution. Considering the length of the jet cooler and the speed of the band, a cooling rate equal to −39.4 °C/s is obtained (see Figure 19), which is the main design parameter for the cooling process.

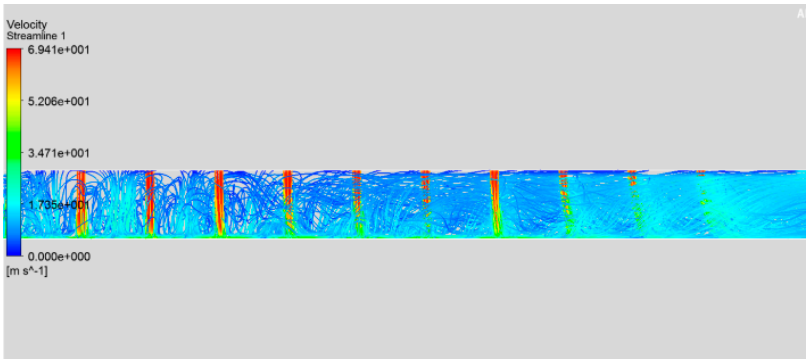

Figure 17. Side view of streamline development.

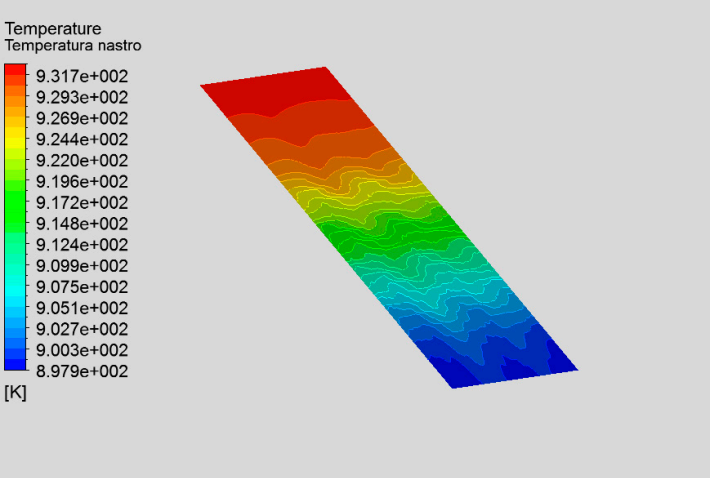

Figure 18. Surface temperature of the band.

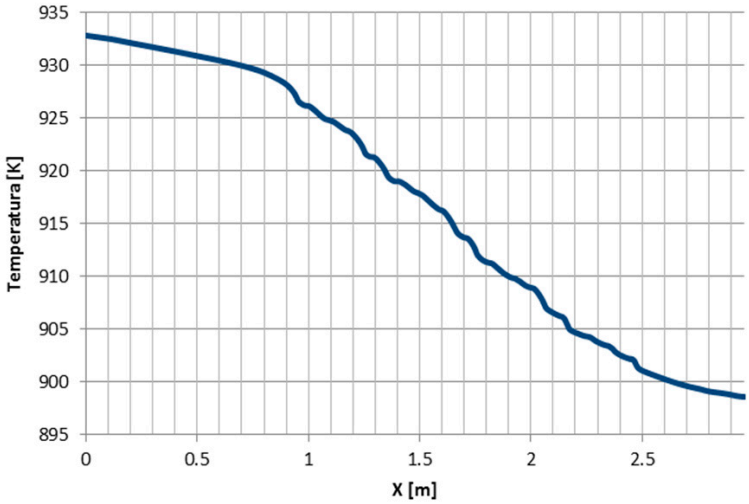

Figure 19. Cooling curve of the band along the midline.

The contours of the heat transfer coefficient along the band are shown in Figure 20. From this image, the difference between the central jets and those closest to the suction is evident; the former are not particularly affected by the adjacent ones due to the rather high values of the jet spacing p_{jet}/D and H/D ratios (where p_{jet} is the pitch distance between the jet centers in the rake). The above contours give a regular distribution of the heat transfer coefficient that decreases when moving away from the stagnation area of each single jet. The above structure is no longer valid for the jets close to the suction, whose flow deflection strongly affects the thermal coefficient. These sets of jets are less efficient, as shown by the low values of h in the contours of Figure 20. The distortion of the jet is reflected in a non-regular distribution of the heat coefficient.

3.2. Heat Coefficient from Correlations and CFD

To evaluate the convective thermal exchange coefficient, the radiant heat flux must be taken into account and subtracted from the total flux. The definition of the heat transfer coefficient is:

$$h = \frac{(total\ heat\ flux - radiative\ heat\ flux)}{\left(T_{wall} - T_{jet}\right)} \quad (5)$$

The average value of the convective heat transfer coefficient for the entire belt is 110.359 $\left[\frac{W}{m^2K}\right]$, while for the "impingement" area (i.e., the surface portion of the band below the jets) is 171.327 $\left[\frac{W}{m^2K}\right]$. On the other hand, the radiant heat flux is equal to 13.3% of the total thermal flux on the band. If only the impingement area is considered, the percentage of the radiant heat flux, compared to the overall value, drops to 9.2%. Such a difference is due to the stronger importance of the convective heat exchange in the area where the jets impinge on the band.

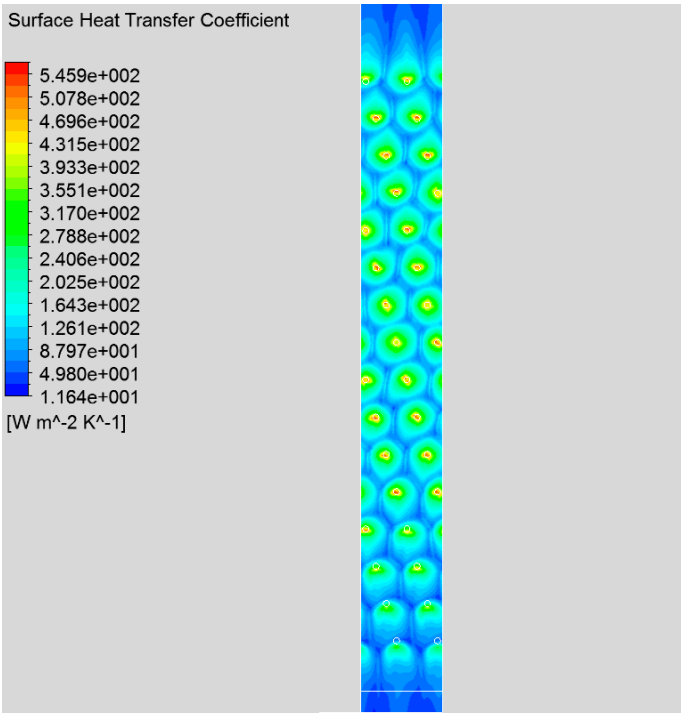

Figure 20. Distribution of the coefficient with convective thermal exchange along the band.

Table 3 compares the results from the CFD with those obtained using the main correlations from the literature, as reviewed by Zuckerman et al. [6] and the proprietary data from Milani [19]. The correlations that have a better match with the numerical results are those of Milani and of Martin and Floreschutz. This is a significant result from the CFD approach in order to be coherent with the industrial design criteria based on correlations.

Table 3. Comparison of numerical results and numerical correlations [6].

	Nu (Average)	Convective Heat Transfer Coefficient h [W/m^2 K]	Percentage Error
CFD	83.39	171.31	—-
Geers (inlet)	102.25	210.06	22.61
Milani (film)	339.55	165.92	−3.15
Floreschutz (film)	53.14	178.51	4.20
Martin (film)	46.65	156.72	−8.25
Huber-Viskanta (inlet)	99.71	204.85	19.57
Huber-Viskanta (film)	49.18	165.22	−3.55
Goldstein-Seol (inlet)	41.30	84.84	−50.47
Goldstein-Seol (film)	20.57	69.12	−59.65

4. Conclusions

The application of CFD analysis on test cases for jet coolers has allowed the setup of a simulation process based on CFD for the accurate prediction of the heat transfer coefficient. The distribution of inlet velocity and turbulence at the jet inlet is a crucial boundary condition that strongly affects the downstream impingement process and its related heat transfer. Separate and specific simulations are therefore required in order to set the proper velocity and turbulence distribution at the jet inlet section. The CFD model has been successfully applied to an industrial cooler module. The simulation setup has been confirmed by overall data from the industrial design. The use of the CFD approach is twofold:

- to calibrate the heat transfer correlations available in the literature for the specific industrial design layout;
- to give a detailed insight into the jet impingement mechanism in the system in order to optimize the heat transfer and reduce, if possible, the mass flow rate of the cooling fluid.

The simulation model can be routinely used for different geometries (for example, by varying the jet–wall distance or the pitch of jets), to check and to compare different layouts, and to identify the most efficient design (highest heat transfer, lowest mass flow rate) for a given plant.

Author Contributions: Conceptualization and Methodology: C.C., G.C., M.M. (Matteo Mazza). Formal analysis: M.M. (Martino Marini). Writing: C.C., M.M. (Martino Marini). All authors have read and agreed to the published version of the manuscript.

Funding: This research received no external funding.

Acknowledgments: Danieli Centro Combustion Spa, Genova provided the reference geometry and data for the industrial configuration. Only a limited set of results has been published due to confidentiality reasons. The technical support from Danieli and the useful discussions during the research activity are warmly acknowledged.

Conflicts of Interest: The authors declare no conflict of interest.

References

1. Basso, D.; Cravero, C.; Reverberi, A.P.; Fabiano, B. CFD analysis of regenerative chambers for energy efficiency improvement in glass production plants. *Energies* **2015**, 88945–88961. [CrossRef]
2. Cogliandro, S.; Cravero, C.; Marini, M.; Spoladore, A. Simulation strategies for regenerative chambers in glass production plants with strategic exhaust gas recirculation system. *IIETA Int. J. Heat Technol.* **2017**, *35*, S449–S455. [CrossRef]
3. Cravero, C.; de Domenico, D.; Leutcha, P.J.; Marsano, D. Strategies for the numerical modelling of regenerative pre-heating systems for recycled glass raw material, mathematical modelling of engineering problems. *IETA* **2019**, *6*, 324–332. Available online: http://iieta.org/journals/mmep (accessed on 28 July 2020). [CrossRef]
4. Cravero, C.; Satta, A. Comparison of semi empirical correlations and a navier-stokes method for the overall performance assessment of turbine cascades. *ASME J. Fluids Eng.* **2003**, *125*, 308–314. [CrossRef]
5. Cravero, C.; Satta, A. A CFD model for real gas flows, ASME Paper 2000-GT-0518. In Proceedings of the ASME Turbo Expo 2000, Munich, Germany, 8–11 May 2000.
6. Zuckerman, N.; Lior, N. Jet impingement heat transfer: Physics, correlations and numerical modeling. *Adv. Heat Transf.* **2006**, *39*, 566–630.
7. Katti, V.; Prabhu, S.V. Experimental study and theoretical analysis of local heat transfer distribution between smooth flat surface and impinging air jet from a circular straight pipe nozzle. *J. Heat Mass Transf.* **2008**, *51*, 4480–4495. [CrossRef]
8. Geers, L.F.G. Multiple Impinging Jet Arrays: An Experimental Study on Flow and Heat Transfer. Ph.D. Thesis, Delft University of Technology, Delft, The Netherlands, 2004.
9. Behnia, M.; Parneix, S.; Durbin, P.A. Prediction of heat transfer in an axisymmetric turbulent jet impinging on a flat plate. *Int. J. Heat Mass Transf.* **1998**, *41*, 1845–1855. [CrossRef]
10. Bovo, M.; Etemad, S.; Davidson, L. On the numerical modeling of impinging jet heat transfer. In Proceedings of the International Symposium. on Convective Heat and Mass Transfer in Sustainable Energy, Yasmine Hammamet, Tunisia, 26 April–1 May 2009.

11. Thielen, L. Modeling and Calculation of Flow and Heat Transfer in Multiple Impinging Jets. Ph.D. Thesis, Delft University of Technology, Delft, The Netherlands, 2003.
12. Pattamatta, A.; Singh, G.; Mongia, H. Assessment of turbulence models for free and confined impinging jet flows. In Proceedings of the 42nd Thermophysics Conference, Honolulu, HI, USA, 27–30 June 2011.
13. Chougule, N.K.; Parishwad, G.V.; Gore, P.R.; Pagnis, S.; Sapali, S.N. CFD analysis of multi-jet air impingement on flat plate. In Proceedings of the World Congress on Engineering, London, UK, 6–8 July 2011; Volume 3.
14. Wae-Hayee, M.; Perapong, T.; Nuntadusit, C. Influence of nozzle arrangement on flow and heat transfer characteristics of arrays of circular impinging jets. *Songklanakarin J. Sci. Technol.* **2013**, *35*, 203–212.
15. ERCOFTAC. Classic Database, Normally-Impinging Jet from a Circular Nozzle. Available online: www.ercoftac.org (accessed on 28 July 2020).
16. ERCOFTAC. Database, Multiple-impinging jets: Flow and heat transfer—Test case 11.4. In Proceedings of the 11th Workshop at Chalmers University of Technology, Gothenburg, Sweden, 7–8 April 2005.
17. Yan, X. A Preheated-Wall Transient Method Using Liquid Crystals for the Measurement of Heat Transfer on External Surfaces and in Ducts. Ph.D. Thesis, University of California, Davis, CA, USA, 1993.
18. Baughn, J.W.; Shimizu, S. Heat transfer measurement from a surface with uniform heat flux and impinging jet. *ASME J. Heat Transf.* **1989**, *111*, 1096–1098. [CrossRef]
19. Milani, A. *Sviluppo Tecnologico dei Forni Continui per i Trattamenti Termici, Scambio Termico per Convezione Nei "Jet-Coolers"*; Internal Report; Danieli Spa: Buttrio, Italy, 2003.